Acta Mech 224, 383–397 (2013)
DOI 10.1007/s00707-012-0755-4

C. Palacios-Morales · R. Zenit

Vortex ring formation for low *Re* numbers

Received: 7 February 2012 / Revised: 18 September 2012 / Published online: 13 November 2012

Abstract The dynamics of formation and evolution of vortex rings with low Reynolds numbers created in a piston-cylinder arrangement are studied. The ratio of the piston displacement L_m to the nozzle diameter D_0 determines the vortex size and evolution. Experiments with different conditions are presented: translation velocity of the piston and stroke ratio L_m/D_0 for $150 < Re < 260$. Measurements of the 2D velocity field were obtained with a PIV technique. The vortex circulation was computed considering a vortex identification scheme (Q criterion). The results show that there is a critical value of L_m/D_0 above which the circulation inside the vortex cannot increase and remains constant. For the Reynolds numbers studied, we found that the limit stroke ratio is $4 \leq L_m/D_0 \leq 6$. As Re decreases, the vortices become "thicker"; therefore, they are able to accumulate more vorticity and increase their circulation.

1 Introduction

In the last thirty years there has been an increased interest in the study of vortex rings. Many of the early works appear in the reviews of Shariff and Leonard [1] and Lim and Nickels [2]. There are many examples of the importance of vortex rings in nature. Many biological flows are characterized by vortex production and vortex shedding. In animal locomotion, the production of coherent structures such as vortex rings is common; these structures have been studied in squid jet propulsion by Anderson and Grosenbaugh [3] as well as Bartol et al. [4,5]. Dabiri et al. [6] studied a species of jellyfish that creates single vortex rings. This kind of vortex can also be seen in internal flows, such as the discharge of blood into the left ventricle of heart (Gharib et al. [7]). Querzoli et al. [8] studied experimentally the motion of vortex rings generated by gradually varied flows which reproduce the characteristics of these biological conditions.

For the case of laminar vortex rings, in particular for those generated by a piston-cylinder arrangement, there are many experimental studies, for instance Maxworthy [9], Didden [10], Glezer and Coles [11] and Weigand and Gharib [12]. The seminal paper of Gharib et al. [13] revived the interest in this subject. They found that the circulation that a vortex ring could attain was finite: There was a maximum amount of fluid vorticity that could be contained within a ring. The parameter that determined whether the circulation had reached a maximum was the "formation time" $t^* = U_p t/D_0$, where U_p is the mean piston velocity, t ($0 \leq t \leq T_0$) is the discharge time, and D_0 is the inner diameter of the cylinder. In particular, $U_p T_0/D_0$ is equal to the stroke ratio L_m/D_0, where T_0 is the total discharge time and L_m is the total piston displacement. They found that for values smaller than $L_m/D_0 \approx 4$, a solitary vortex ring was formed, while for larger values of L_m/D_0, a leading vortex followed by a trailing jet and secondary vortices was observed. The circulation contained within the leading vortex ring could not be further increased even if L_m/D_0 kept on increasing. The critical value of L_m/D_0 for which

C. Palacios-Morales · R. Zenit (✉)
Instituto de Investigaciones en Materiales, Universidad Nacional Autónoma de México,
Circuito Exterior, Ciudad Universitaria, 04510 Mexico, DF, Mexico
E-mail: zenit@unam.mx

the transition between these two states occurs was called the "formation number." For the vortex-trailing jet regime, the vortex ring circulation was computed after the vorticity field of the leading vortex ring had been completely disconnected from that of the trailing jet. For different experimental configurations Gharib et al. [13] found that the formation number lies in the range of 3.6–4.5.

Some authors have discussed that the value of the formation number may vary because of different factors: changes in the piston velocity program (acceleration) [14], the cylinder exit velocity profile [15] or, more recently, the existence of an imposed bulk counterflow [16] and a background co-flow [17]. In particular, Linden and Turner [18] discussed that the maximum value of L_m/D_0 above which a single ring cannot be formed may be as large as 7.83. By temporally varying the exit cylinder diameter during formation, Dabiri and Gharib [19] observed that the formation number could be delayed up to 8. Based on the study of a jellyfish swimming kinematics, Dabiri et al. [6] reported that the limiting vortex formation time was delayed to at least 8. Following Rosenfeld et al. [15], we define the Reynolds number as follows:

$$Re_0 = \frac{D_0 U_{\max}}{\nu} = \frac{D_0 U_p}{\nu}, \tag{1}$$

where ν is the kinematic viscosity and $U_{\max}$ is the maximal piston velocity; for an impulsive velocity program, $U_{\max} \approx U_p$. The main purpose of the present investigation is to explore the vortex ring formation process for Re_0 of O(100). For such low Reynolds numbers, a physical separation between the leading vortex ring and the trailing jet does not occur. For this reason, the procedure to compute the vortex circulation previously used for flows with higher Re_0 is not appropriate. Based on Eq. (1), Gharib et al. [13] presented results of flows with $Re_0 = 1{,}905$ and $Re_0 = 3{,}810$. Hence, we propose an alternative method based on the so-called Q criterion to identify the vortex ring and measure its circulation.

In the present investigation we analyze the formation process of vortex rings for a range of Re_0 in between 150 and 260. In accordance with the previous investigations, we found that the vortex rings attain a maximum circulation for a critical value of the stroke ratio. We discuss our results to justify these findings. To our knowledge, measurements of the formation process of vortex rings for Re_0 of O(100) do no exist in the literature. We also propose a procedure to improve the location of vortex ring centers by computing the curvature of Lagrangian trajectories in the flow.

2 Determination of vortex ring properties

2.1 Vortex identification

Notwithstanding vortices have been studied for a long time, there is not a consensus of a mathematical definition of a vortex in the fluid mechanics community. Different definitions are based on vorticity limit values, pressure minima, closed pathlines or streamlines. Jeong and Hussain [20] discuss the problems of using these definitions. Normally, a vortex is associated with a region of flow with high vorticity; however, there is no universal threshold over which the vorticity value is to be considered high [21]. In real fluids, the diffusion of vorticity by viscosity impedes the existence of a sharp boundary between rotational and irrotational flow.

The most widely used schemes to identify vortices are based on the local analysis of the velocity gradient tensor $\nabla \boldsymbol{u}$ [22]. Examples of these Galilean invariant techniques are the Q criterion of Hunt et al. [23], the λ_2 criterion of Jeong and Hussain [20] and the Δ criterion proposed by Chong et al. [24]. The analysis of $\nabla \boldsymbol{u}$ provides a rational basis for vortex identification and the general classification of 3D flow fields [24]. In particular, Querzoli et al. [8] used the Δ criterion to obtain the vortex rings area on the measurement plane. For two-dimensional flows, the Q criterion is known as the *Okubo–Weiss* criterion proposed by Okubo [25] and Weiss [26]. The Q criterion uses the velocity gradient decomposition:

$$\nabla \boldsymbol{u} = \boldsymbol{S} + \boldsymbol{\Omega}, \tag{2}$$

where $\boldsymbol{S} = \frac{1}{2}((\nabla \boldsymbol{u}) + (\nabla \boldsymbol{u})^t)$ is the symmetric and $\boldsymbol{\Omega} = \frac{1}{2}((\nabla \boldsymbol{u}) - (\nabla \boldsymbol{u})^t)$ the antisymmetric component of $\nabla \boldsymbol{u}$. The second invariant Q for an incompressible flow is defined as

$$Q = \frac{1}{2}(|\boldsymbol{\Omega}|^2 - |\boldsymbol{S}|^2), \tag{3}$$

where $|\boldsymbol{\Omega}| = tr[\boldsymbol{\Omega}\boldsymbol{\Omega}^t]^{1/2}$ and $|\boldsymbol{S}| = tr[\boldsymbol{S}\boldsymbol{S}^t]^{1/2}$. Where $Q > 0$, the local measure of rotation rate is larger than the strain rate; therefore, the spatial region belongs to a vortex. This function can be evaluated point-by-point,

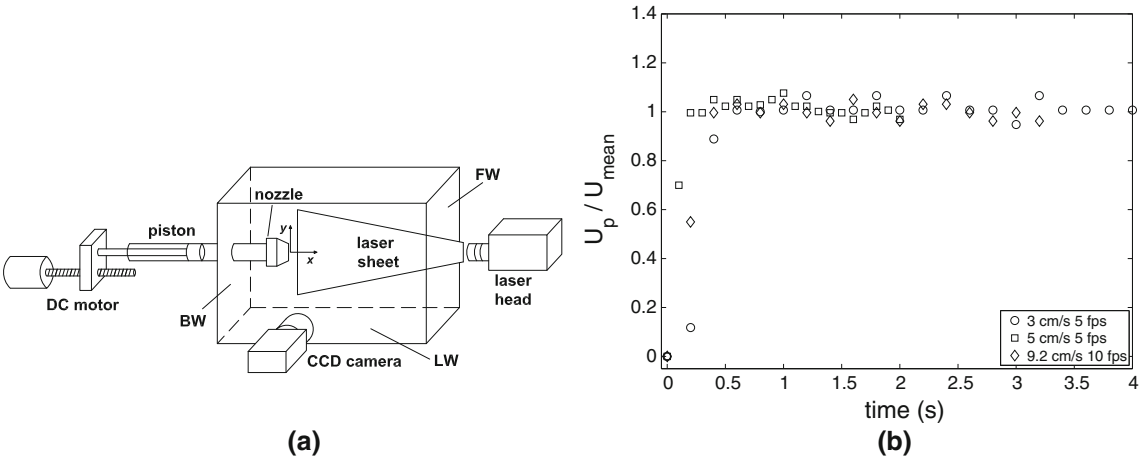

Fig. 1 **a** Experimental setup, **b** Piston velocity programs for different voltages

and we can classify each point as being inside or outside the vortex ring. With this procedure, the vorticity within the core of the vortex can be quantified without having to choose a vorticity threshold.

2.2 Vortex ring center

We use a method to find topologically relevant points in the flow to locate the vortex ring center. In a two-dimensional flow, special points can be found in the regions where the local velocity becomes zero [27]. There are two types of special points. When located in a region of the flow where the vorticity dominates, such points are elliptic; in a strain-dominated region, they are hyperbolic (i.e., saddlelike). It has been shown that the elliptical points correspond to the center of the vortices in the flow [24]. It is possible to find the elliptic and hyperbolic points by computing the curvature of Lagrangian trajectories, that is, the trajectories of individual moving fluid elements; in this case, we use the 2D velocity field obtained by the PIV technique. Near both hyperbolic and elliptic points, the direction of fluid particle trajectories changes over very short length scales, producing large curvature values. The curvature was obtained following the scheme of Braun et al. [28]:

$$k(t) = \frac{|\boldsymbol{u} \times \partial_t \boldsymbol{u} + \boldsymbol{u} \times [\boldsymbol{u} \cdot \nabla \boldsymbol{u}]|}{|\boldsymbol{u}|^3}, \tag{4}$$

where **u** is the velocity field and ∂_t is the partial time derivative. Once the points of local maximum curvature are identified, it is possible to classify them as elliptic or hyperbolic using the Q criterion described above. If the special point has a Q value $Q < 0$, the local flow is dominated by strain; if $Q > 0$, where rotation dominates, the point is the center of a vortex ring. It is important to note that the time resolution of our experiments (15 Hz) is sufficient to compute the temporal term (as discussed later).

3 Experimental setup

Figure 1a shows the experimental setup. Experiments were performed in a tank using a piston-cylinder arrangement. Vortex rings were generated by the displacement L of a piston inside the cylinder of diameter D_0. The tank and cylinder are made of plexiglass. The tank dimensions were as follows: $70 \times 30 \times 30$ cm. The cylinder is 40 cm long and is set horizontally at the center of the tank. The inner diameter is $D_0 = 25.7$ mm. A sharp-edged cylindrical nozzle was coupled at the end of the cylinder. The tip angle of the nozzle is $\alpha = 20°$, and the exit diameter is also 25.7 mm. The nozzle exit was placed 25 cm ($7.8D_0$) from the back wall (BW), 15 cm ($5.8D_0$) from lateral walls (LW) and 45 cm ($17.5D_0$) from the front wall (FW). The x-axis coincides with the centerline of the nozzle, and the nozzle-exit plane is located in the plane $x = 0$.

The driving mechanism consists of the following. The piston was coupled with a stem which was pushed through by a screw, coupled to a DC motor. The mean piston velocity U_p was proportional to the supplied voltage. The DC power supply was controlled by a computer using LabView®. Therefore, it was possible to

control and fix the piston velocity and the piston displacement. If the desired displacement was $L_m = nD_0$ where $n = 1, 2, \ldots, 10$, the piston moved a distance x_m so $|x_m - L_m| / L_m \leq 0.02$. Different velocities and displacements of piston were used. The maximum mean piston velocity was $U_p \approx 20$ cm/s, and the maximum displacement was $L_m = 10$. In Fig. 1b we present three different piston velocity programs normalized with the mean velocity. In these tests, we measured the piston velocity by calculating its displacement between consecutive frames obtained with a digital camera at different frame rates (fps). We can observe that the piston velocity program was impulsive and the mean piston velocity was reached at approximately 0.25 s; the error of these measurements is 5 %.

In order to keep the Reynolds number small, three different aqueous solutions of polyethylene glycol (PEG) were used. The PEG used in the present investigation has a molecular weight of 20,000 g/gmol and is fabricated by Clariant®. The smallest Reynolds number, $Re_0 = 150$, is a 6 % weight PEG solution with viscosity $\mu = 8$ mPa s and density $\rho = 1.07$ g/cm^3 at 23 °C, while the mean piston velocity for this case was $U_p = 4.8$ cm/s. For $Re_0 = 200$ we used the same liquid and increased the mean piston velocity to $U_p = 7.70$ cm/s. For $Re_0 = 260$ we increased the PEG concentration as well as the piston velocity to have $\mu = 12.7$ mPa s and $U_p = 16$ cm/s. To measure the viscosity we used a Brookfield® DV-III viscometer; the density was measured using a pycnometer and an analytical balance.

Two-dimensional velocity fields were obtained using the particle image velocimetry technique (PIV), using a Dantec Dynamics system. A Nd:YAG laser system generates a 50 mJ energy 532 nm laser beam which was converted to a laser sheet using optics. The laser sheet illuminated a vertical slide at the center of the cylinder. A CCD camera was positioned to record images illuminated by the laser sheet. The resolution of the camera was 1,008 × 1,016 pixels, and the typical measurement area was 141 × 142 mm^2. Neutrally buoyant silver-coated glass spheres with an average diameter $10 \pm 5\mu m$ were used as particle tracers. The velocity field consisted of 62 × 62 vectors using an interrogation area of 32 × 32 pixels and an overlap of 50 %. The spatial resolution was 2.24 × 2.24 mm^2 for most of the experiments, and the sampling rate was 15Hz. A detailed description of the PIV technique can be found in [29] and [30].

3.1 Measurements uncertainties

Several authors have analyzed the uncertainty in the measurements of velocity gradients obtained by PIV and other optical techniques because the calculation of these quantities depends on the spatial derivatives of the measured velocity [31–33]. Following the procedure proposed by Kline and McClintock [32], the uncertainty in the measurement of the velocity gradient tensor $\nabla \boldsymbol{u}$ can be calculated as:

$$\frac{\delta \nabla \boldsymbol{u}}{\langle \nabla \boldsymbol{u} \rangle} = \left[\left(\frac{\delta U}{\langle U \rangle} \right)^2 + \left(\frac{\delta \lambda}{\langle \lambda \rangle} \right)^2 \right]^{1/2}, \tag{5}$$

where δU, $\delta \lambda$, $\langle U \rangle$ and $\langle \lambda \rangle$ are the uncertainty and mean value of the velocity and length, respectively. $\langle \nabla \boldsymbol{u} \rangle$ is the measured value of the velocity gradient tensor. Considering relative uncertainties of 4 % in both velocity and length, a maximum value of $\delta \nabla \boldsymbol{u} / \langle \nabla \boldsymbol{u} \rangle \approx 5.6$ % is expected. Lourenco and Krothapalli [33] suggested that the truncation error is also important in the computation of velocity gradients. This error can be obtained by the expression [31]:

$$T_{ij} = -\frac{1}{6} \frac{\partial^3 u_i}{\partial x_j^3} (\delta x_i)^2, \tag{6}$$

where the repeated indices do not imply summation. Using Eq. (6) it is possible to obtain the maximum truncation error in a vector field map. In our case, we have measured that $(T_{ij})_{\max} / (\langle U \rangle / \langle \lambda_{\max} \rangle) \approx 0.017$, where $\lambda_{\max}$ is the mesh distance (spatial resolution) and $\langle U \rangle$ is the modulus of the velocity vector for which T_{ij} is maximum. Following the arguments proposed by Ozcan et al. [31], we estimate that the uncertainty of the measurement is roughly twice the truncation error; hence, $\delta \nabla \boldsymbol{u} / \langle \nabla \boldsymbol{u} \rangle \approx 3.4$ % considering only the truncation error. Hence, the total error in the measurement of the velocity gradient is below 6 %.

4 Results

Figure 2 shows the velocity, vorticity and the Q criterion fields (top, middle and bottom rows, respectively) of two flow cases, both at $Re_0 = 260$. The first one (Fig. 2 a, b, c) corresponds to the production of a single and isolated vortex ring. This configuration occurs for a relatively small stroke ratio; in this case $L_m/D_0 = 3$. The second case (Fig. 2 d, e, f) corresponds to a flow for which a leading vortex ring followed by a trailing jet was observed. This regime results for larger L_m/D_0 (in this case $L_m/D_0 = 8$). Both vortices are located at a position of $x \approx 5D_0$. Different experimental condition (exit diameters, exit plane geometries and non-impulsive piston velocities) carried out by Gharib et al. [13] showed that the transition between the two regimes occurs when $L_m/D_0 \approx 4$.

The vorticity field of Fig. 2b shows that most of the vorticity in the flow is concentrated in the vortex ring area. This means that the vorticity generated in the boundary layer inside the cylinder was introduced into the vortex ring. On the other hand, the vorticity field for the case $L_m/D_0 = 8$ shows a trailing shear layer connected with the leading vortex ring. The process of separation between the vortex ring and trailing jet can occur at different distances depending on the stroke ratio [15]; however, for our experiments ($Re_0 < 260$), the leading vortex ring never "disconnects" from its trailing jet. Dabiri [34] pointed out that the physical separation is not to be confused with the vortex ring "pinch-off" which is the process whereby a forming vortex ring is no longer able to entrain additional vorticity; the separation may occur later or not at all. Most authors have limited the size of the vortex ring by choosing an arbitrary minimum vorticity contour value or a percentage of the maximum vorticity at the vortex core. In our case, such criteria become subjective since the separation between the vorticity fields of both the vortex ring and the trailing jet is not evidently observable.

Figures 2c and 2f show the Q fields for the previous cases. For the single vortex ring case we observe that the region of high rotation rate ($Q > 0$) coincides with the core of the vortex ring. The plot shows that this area is smaller than the corresponding vorticity field. The Q criterion map for the case $L_m/D_0 = 8$ shows a remarkable separation between the vortex ring and the trailing jet. In fact, it is possible to locate secondary vortices behind the leading one. We can also observe strain-dominant regions of the flow (negative Q values, indicated by the dashed lines in the figure) which are located mainly in front of the leading vortex ring. Based on these observations, we will consider the area of the vortex ring to be that for which $Q > 0.01\,\mathrm{s}^{-2}$ for all cases. This Q value represents the uncertainty within which this quantity can be measured.

Figure 3 shows the location of points of maximum curvature (circles), and maximum (or minimum) vorticity (squares) for $Re_0 = 150$. The stroke ratio is $L_m/D_0 = 4$, and the position of the vortex center (considering maximum curvature) is $x \approx 8D_0$. Contours of constant curvature (a) and constant vorticity (b) are shown in solid black lines. The minimum and maximum contour values of curvature are $150\,\mathrm{m}^{-1}$ and $3{,}000\ \mathrm{m}^{-1}$ (vortex center), respectively. The minimum vorticity value is $0.5\ \mathrm{s}^{-1}$, and the maximum absolute vorticity value is $1.8\,\mathrm{s}^{-1}$. To calculate vorticity and curvature scalar maps (and also peak values), we first constructed a subgrid of $\Delta x/3$ and $\Delta y/3$ ($\backsim 0.75$ mm) nodes, and then the velocity field was interpolated to fit the subgrid using triangle-based linear interpolation. The temporal term $\boldsymbol{u} \times \partial_t \boldsymbol{u}$ from Eq. (4) was obtained using a central difference computation, that is, we considered the previous and following vector maps. However, it was also possible to compute the curvature without this temporal term obtaining differences (in the peak curvature) lower than 0.8 % in the axial direction. If x is the distance desired to locate the vortex ring (say $x = 8D_0$), we found a maximum error of $|x - x_k|/x \leq 3\,\%$ (where x_k is the vortex position measured with peak curvature) but typically less than 1 %. Vector fields from Fig. 3 are resampled for clarity. It is important to note that in most of our experiments the maximum vorticity coincides with the maximum Q value, that is, the region of the flow with high rotation rate. However, the point of maximum vorticity does not necessarily coincide with the point of maximum curvature. In general, the point of maximum vorticity tends to move toward the axis of symmetry where velocity gradients are higher; this difference is more noticeable as Re_0 decreases. We observe that in fact the maximum point of curvature better locates the geometric centers of the vortex ring than the maximum vorticity point, that is, the maximum curvature is located closer to the azimuthal axis (rotation axis) of the vortex ring. It is important to note that the vortex presented in Fig. 3 is located at a distance in which the vortex circulation has already achieved its maximum value; *ergo*, the vortex ring has completed its formation. Some previous publications [35] indicate that it is possible to have vortical structures with extremum value of vorticity outside the rotation axis. The so-called hollow vortices are characterized by a slowly rotating center (weak vorticity), surrounded by a high-speed circumferential jet (strong vorticity). These vortices have been observed in nature, specifically in geophysical flows like the Antarctic Stratospheric vortex (ozone hole) and the Great Red Spot(GRS) on Jupiter [36]. We also observe that vortex rings tend to broaden as Re_0 decreases.

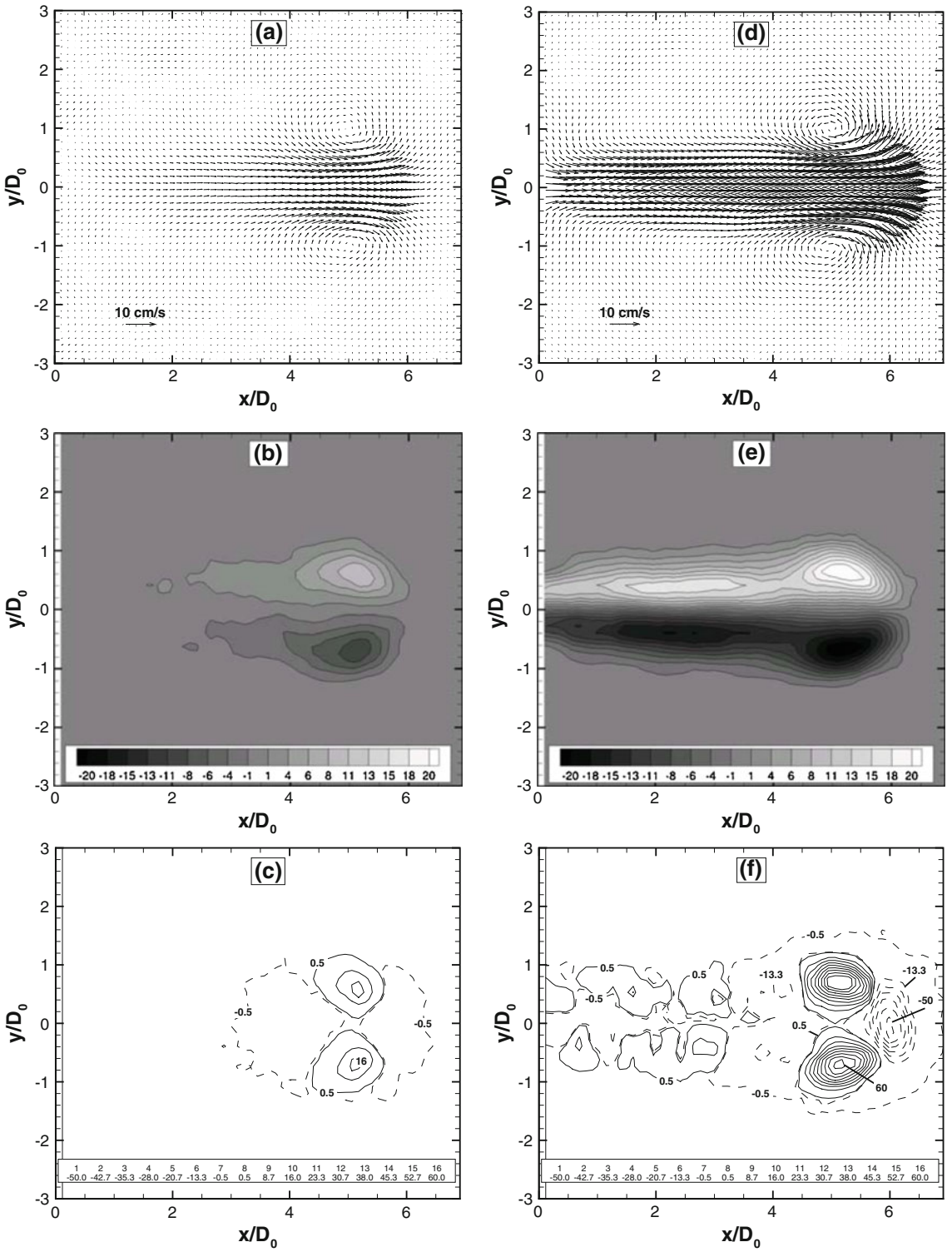

Fig. 2 Velocity, vorticity and Q criterion fields for $Re_0 = 260$. $L_m/D_0 = 3$ (*left*) and $L_m/D_0 = 8$ (*right*). Vortex position at $x \approx 5D_0$. Vorticity in s^{-1} and Q values in s^{-2}

Figure 4 shows the vortex ring trajectory considering the points of maximum curvature and maximum vorticity for stroke ratio $L_m/D_0 = 8$ and two different Reynolds numbers. In this graph, the position of the vortex ring center on the upper half plane ($y > 0$) is plotted. The points of maximum curvature ($k_{\max}$) are

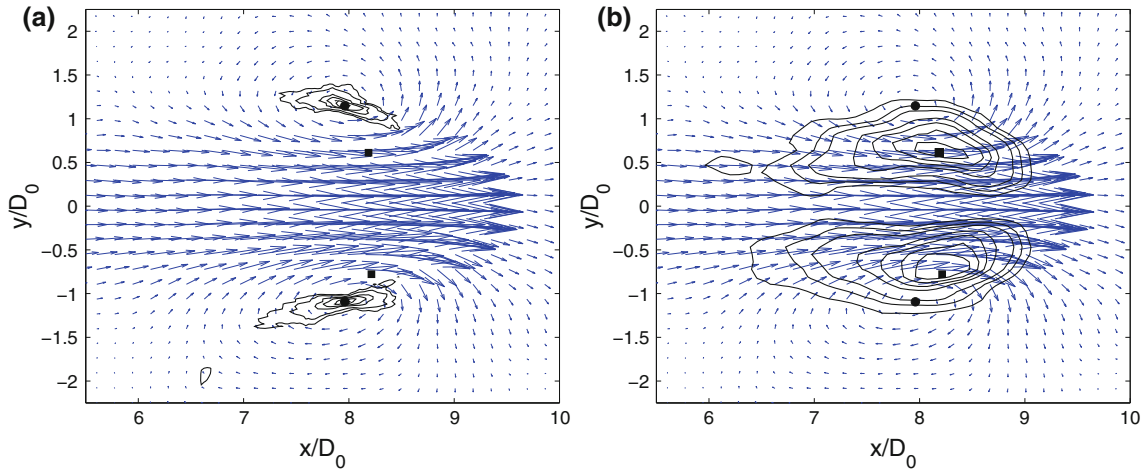

Fig. 3 Comparison between points of **a** maximum curvature (*filled circle*) and **b** maximum (or minimum) vorticity (*filled square*). $L_m/D_0 = 4$, $x \approx 8D_0$ and $Re_0 = 150$

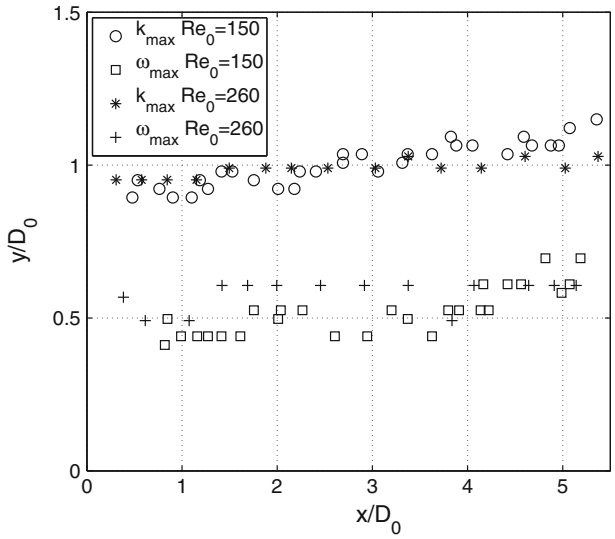

Fig. 4 Trajectory of vortex ring center considering maximum curvature and maximum vorticity for $L_m/D_0 = 8$

located at a distance $y/D_0 \approx 1$ for both Reynolds numbers, while the points of maximum vorticity are close to $y/D_0 = 0.5$. As mentioned before, the maximum vorticity locates closer to the axis of symmetry. For a given L_m/D_0, Weigand and Gharib [12] found that the trajectories of the vortex rings centers are spatially independent of the Reynolds number, in agreement with our results presented in Fig. 4. For all the results presented in this paper, the vortex ring position is obtained from the point of maximum curvature.

Figure 5 shows the evolution of the non-dimensional vortex ring diameter D_v/D_0 for different stroke ratios and $Re_0 = 260$. D_v is the distance between centers of the upper and lower half plane located from the points of maximum curvature; x_m is the mean x position of the centers. The results indicate that the vortex ring diameter increases in the axial direction, which has been reported in several previous works. Didden [10] found that for $L_m/D_0 \leq 2$ the vortex diameter increases with the stroke ratio, which is consistent with our experimental results. We found, however, that when $L_m/D_0 \geq 4$ (and $Re_0 = 260$), the vortex diameter initially increases and then remains constant with a value close to $2D_0$. This indicates that the vortex ring reaches a limit size even though the stroke ratio keeps on increasing. Gharib et al. [13] pointed out this constraint in their flow visualizations. As the leading vortex ring loses its strength, it decelerates in the x direction and the diameter may increase even more. For low stroke ratios, Didden [10] reported a sudden decrease in the ring diameter after the end of each stroke. We observe the same phenomenon in Fig. 5 for $L_m/D_0 = 1$ and

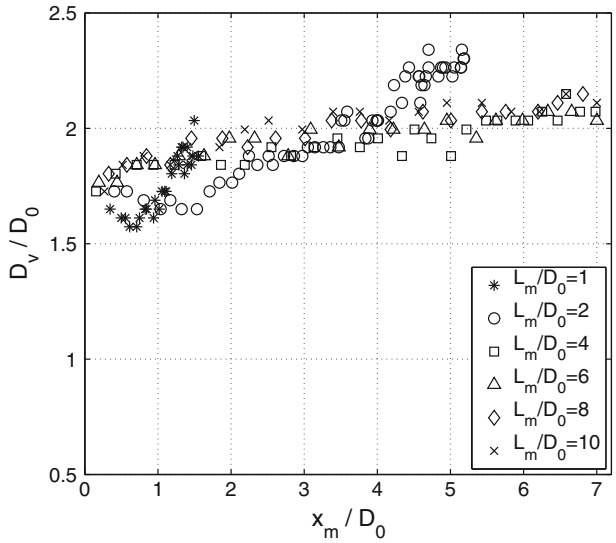

Fig. 5 Vortex ring diameter for different stroke ratios. $Re_0 = 260$

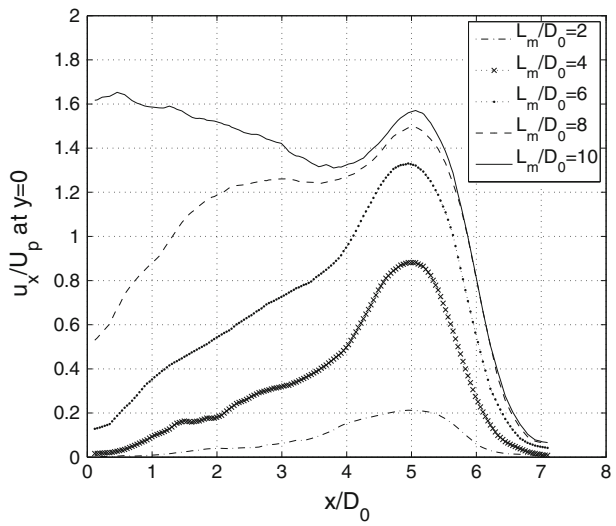

Fig. 6 Horizontal velocity profile at $y = 0$ for different stroke ratios. Vortex ring center at $x = 5D_0$. $Re_0 = 260$

$L_m/D_0 = 2$. It is important to note that the vortex ring diameters presented in Fig. 5 could be slightly different from those reported in the previous works; for instance, Didden [10] presented $D/D_0 = 1.1$–1.4 for rings with $L_m/D_0 = 2$. This difference results from the way through which the vortex ring center is located, in our case the maximum curvature points. Didden measured the vortex ring diameter using dye visualization images (movie films). If we consider the maximum vorticity points as the vortex centers, the vortex diameters for $Re_0 = 260$ and $L_m/D_0 = 2$ would be $Dv/D_0 = 0.9$–1.2.

The horizontal liquid velocity profiles (u_x) at $y = 0$ (axial line) are presented in Fig. 6 for different stroke ratios. For all cases the piston velocity is $U_p = 16$ cm/s, and the vortex ring is located at $x = 5D_0$, corresponding to a Reynolds number of $Re_0 = 260$. The plot indicates that the u_x velocity is maximum at the x location of the vortex ring center (considering the maximum point of curvature). We also observe the presence of the trailing jet behind the vortex ring, which appears in our experiments approximately when $L_m/D_0 \geq 4$. This is consistent with Gharib's experiments; however, as was mentioned before, at this Reynolds number the shear layer does not separate from the vortex ring, that is, the vorticity fields of both the vortex and the shear layer remain connected by iso-vorticity lines. It is important to note that the horizontal velocity profile for $L_m/D_0 < 4$ becomes symmetric as Re_0 approaches O(1000). In our case, the solitary vortex ring broadens

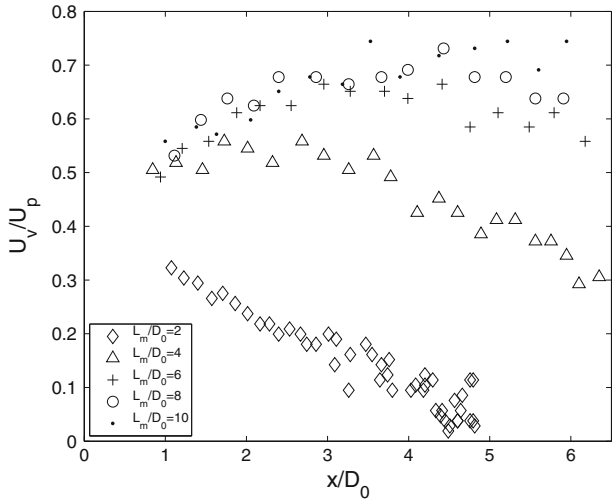

Fig. 7 Propagation velocity of vortex rings for different stroke ratios $Re_0 = 260$

to seemingly form a trailing jet (see, e.g., $L_m/D_0 = 2$ in Fig. 6). During the piston movement, there is an acceleration of u_x velocity at the axial line because of the initial growth of the boundary layer on the cylinder wall; therefore, $u_x/U_p > 1$ for large stroke ratios as shown in Fig. 6.

Figure 7 shows the non-dimensional propagation velocity U_v of vortex rings for different stroke ratios for $Re_0 = 260$. The vortex ring velocity is obtained by a numerical differentiation of the vortex ring position based on the location of maximum curvature. Didden [10] and Weigand and Gharib [12] indicated that vortex ring velocity decays with time. For small stroke ratios ($L_m/D_0 = 2$) the decay of the propagation velocity is important. When the stroke ratio is relatively large $L_m/D_0 \geq 6$, the vortex ring velocity initially is approximately $0.5U_p$ and then it increases slightly as the vortex ring moves away from the nozzle to reach a maximum of $0.7U_p$ approximately; however, a vortex ring velocity decay is expected for larger distances from the nozzle. The velocity for $L_m/D_0 = 4$ remains constant close to $0.55U_p$ before decaying at $x \approx 4D_0$. In their analytical model Mohseni and Gharib [37] predicted a propagation velocity $U_v = 0.5U_p$, which is close to this particular stroke ratio. Querzoli et al. [8] reported the vortex propagation velocity for different piston velocity programs (gradually varying flows). The Reynolds numbers are in the range $7.4 \times 10^3 \leq Re \leq 1.5 \times 10^4$. After an initial increase, the vortex travel velocity reaches a constant non-dimensional value in the range $0.6 \leq U_v/u_*(t_a) \leq 0.8$ depending on the velocity program. The velocity $u_*(t_a)$ is related to the integrated velocity $U_0(t)$ at the orifice exit over the time t_a, when the piston acceleration phase ends. The results presented by [8] agree with the velocity values of Fig. 7 for relatively large stroke ratios despite the Reynolds number differences. For $L_m/D_0 \leq 4$ the vortex propagation velocity rapidly decreases because of viscous effects.

Figure 8 shows the non-dimensional vortex ring circulation as function of the distance x/D_0 from the nozzle-exit plane. The Reynolds number is $Re_0 = 150$. In the present investigation, we used the Q criterion to obtain closed areas to integrate the vorticity and compute the vortex ring circulation, similar as [8]. The circulation is obtained using the formula:

$$\Gamma = \int_{A_Q} \omega_z \mathrm{d}A, \tag{7}$$

where ω_z is the vorticity

$$\omega_z = \frac{\partial u}{\partial y} - \frac{\partial v}{\partial x}, \tag{8}$$

and A_Q is the region of flow where $Q > 0$ (for our calculations we consider $Q \geq 0.01\mathrm{s}^{-2}$). Note that considering this method to measure the circulation, only the vorticity in the core of the vortex is considered. Thus, the circulation values presented here may be lower than those reported by others [13–15]. The points plotted correspond to the average of five different runs of the piston. The error bars represent the standard deviation of the data. It can be observed from Fig. 8 that the vortex circulation grows as the vortex moves

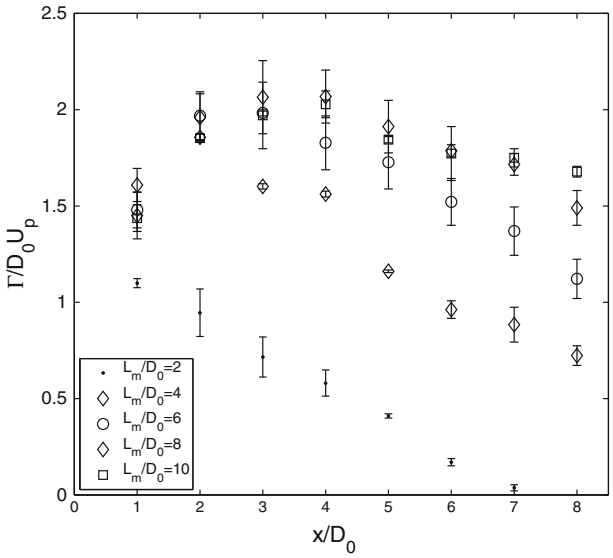

Fig. 8 Non-dimensional vortex ring circulation at different distances from the nozzle. $Re_0 = 150$

away from the nozzle until it reaches a maximum value after which it decreases. This basically means that the vortex ring is initially fed of vorticity until it attains a saturation condition in which the vortex is not able to accumulate more vorticity in its core. Beyond a certain distance the vortex circulation decreases because of vorticity dissipation. In general, the larger the stroke ratio, the larger is the vortex circulation for a given distance from the nozzle. For this particular Re_0 number and when $L_m/D_0 > 4$, the maximum circulation values are reached at a distance between $3D_0 \leq x \leq 5D_0$ which is markedly close to the exit. Moreover, for low stroke ratios, that is, $L_m/D_0 = 2$, the vortex circulation begins to decrease beyond $x \approx D_0$. In contrast, for Re_0 of O(1000) Gharib et al. [13] presented constant ring circulation values at a distance close to $x \approx 10D_0$. The faster decay of circulation is due to the increased dissipation of flows with $Re_0 \sim$ O(100).

Querzoli et al. [8] reported experimental results ($7.4 \times 10^3 \leq Re \leq 1.5 \times 10^4$) of the non-dimensional vortex circulation for different piston velocity programs. The vortex circulation was obtained by integrating the vorticity over the vortex area (identified by the ∇ criterion [24]) and made dimensionless using the scale $u_*(t)D_0$. After an initial increase, Querzoli et al. [8] observed that the vortex circulation reached a constant value (plateau) ranging from 1.5 to 3 depending on the velocity program. In our case, the limiting vortex circulation value is close to 2 (see Fig. 10). They also derived simple predictions of the vortex circulation behavior based on the slug model (Shariff and Leonard [1]) to compare their results. The limiting constant values for most velocity programs (1.5–2.5) predicted by [8] are in close agreement with our experimental results. This means that the scale D_0U_p is good enough for an impulse velocity program regardless of the Reynolds number value. Moreover, in agreement with their predictions, the vortex velocity behavior is very similar as the vortex circulation. In our case, the Reynolds number of the vortices rings is relatively low; thus, the vortex circulation does not remain constant for a long time; instead, it decreases faster because of viscous dissipation.

Figure 9 shows the vortex ring circulation as a function of the stroke ratio L_m/D_0 for $Re_0 = 150$. The curves correspond to different vortex ring positions. For clarity we present only some of the total distances obtained. We can observe that the maximum vortex ring circulation for each stroke ratio is reached at different distances from the nozzle; the same trend has been reported by Rosenfeld et al. [15]. Evidently, the larger the stroke ratio, the farther the distance in which the vortex ring achieves its saturation. Besides the stroke ratio, the Reynolds number may play a role in the distance or time at which the maximum vortex ring circulation is achieved. For the Reynolds numbers studied in this investigation, the maximum values of vortex circulation are achieved at a distance between $4D_0 \leq x \leq 7D_0$. From Fig. 9 we observe that the maximum vortex circulation, for $Re_0 = 150$, is obtained when $L_m/D_0 \approx 4$. The maximum non-dimensional circulation value is close to $\Gamma/D_0U_p \approx 2$.

If we consider the maximum circulation value for each stroke ratio regardless of the distance at which this value is reached, we obtain the plot shown in Fig. 10. In this graph we present three different Reynolds numbers and the experimental results from Gharib et al. [13] (shown in their Fig. 6). Considering the piston

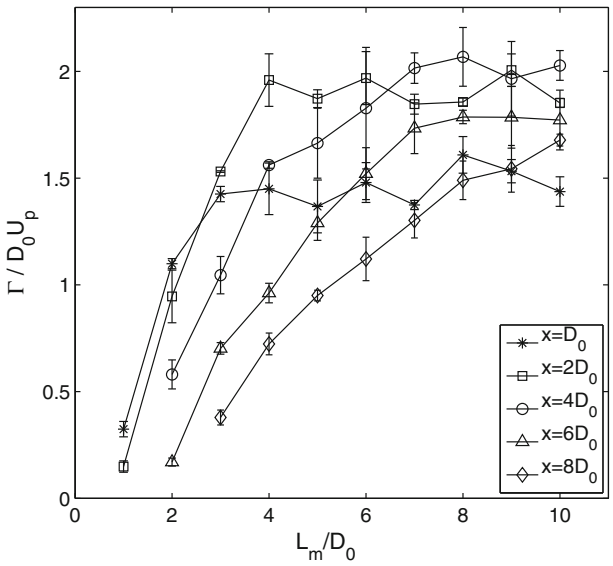

Fig. 9 Non-dimensional vortex ring circulation as a function of the stroke ratio at different distances from the nozzle $Re_0 = 150$

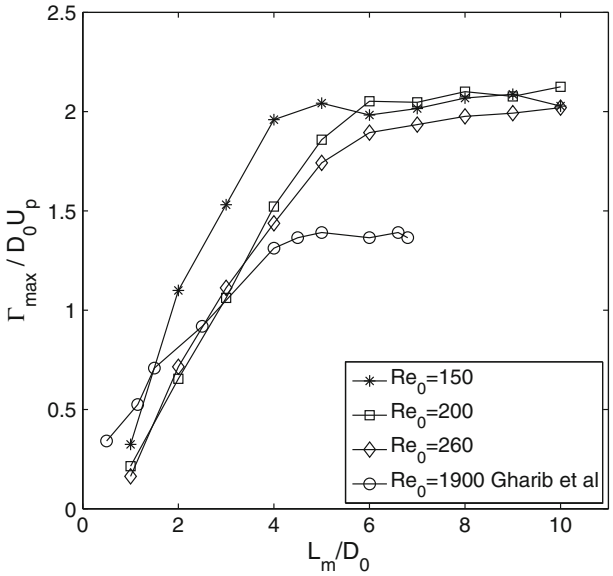

Fig. 10 Maximum vortex ring circulation for each L_m/D_0

mean velocity and the cylinder diameter, the Reynolds number of the data presented from Gharib et al. is $Re_0 = 1{,}905$. For the lower Reynolds number $Re_0 = 150$, we observe that the maximum circulation value is reached when the stroke ratio $L_m/D_0 \approx 4$; for $Re = 200$ and $Re = 260$ the stroke ratio is $L_m/D_0 \approx 6$. We can observe that these limit stroke ratio values are close to those reported by Gharib et al. [13] for $Re_0 = 1{,}905$. For each L_m/D_0, Gharib et al. computed the maximum vortex ring circulation by integrating the vorticity within and iso-vorticity contour of 1 s^{-1}. For these results, they did not specify the exact distance where the vortex ring circulation was measured; however, for $L_m/D_0 > 4$ they measured the vortex ring circulation at a distance beyond which "... a clear separation between vorticity contours of the vortex from those of the trailing jet existed." For all the Reynolds numbers studied, the maximum non-dimensional circulation value is approximately $\Gamma/D_0U_p = 2$. This suggests that at this value the leading vortex ring has reached a saturation condition beyond which it is not possible to attain more vorticity, in agreement with the previous publications.

For the case $Re_0 = 150$ and $L_m/D_0 < 4$, we observe that the vortex circulation is significantly larger than the other Re_0. We will discuss this further in the next section.

5 Discussion

We would like to compare our experimental results to those obtained by the previous analytical studies. Mohseni and Gharib [37] and Linden and Turner [18] proposed models based on matching the properties of the ejected fluid to the corresponding properties of a family of finite-core vortices studied by Fraenkel [38] and Norbury [39]. The effect of viscosity was considered negligible. The properties of the ejected fluid plug were based on the slug flow approximation (Shariff and Leonard [1]). The circulation Γ_p, the impulse I_p and the kinetic energy E_p of the plug fluid are defined as follows:

$$\Gamma_p = \frac{1}{2} U_p L_m, \tag{9}$$

$$I_p = \frac{1}{4} \pi U_p D_0^2 L_m, \tag{10}$$

$$E_p = \frac{1}{8} \pi c U_p^2 D_0^2 L_m, \tag{11}$$

where c is the fraction of the nominal kinetic energy of the plug of fluid actually injected into the ring.

The vortex rings studied by Norbury [39] have vorticity ω_ϕ (in cylindrical coordinates) proportional to the distance r from the axis of symmetry. He classified these rings in terms of a non-dimensional mean core radius ϵ defined by the equation:

$$\epsilon^2 = \frac{A_R}{\pi X_R^2}, \tag{12}$$

where A_R is the area of the vortex ring core and X_R is the ring radius (see Fig. 1 from Norbury [39]). The values of ϵ are in the range $0 < \epsilon \leq \sqrt{2}$, extending from a vortex ring with small cross section (where $\epsilon \to 0$) to Hill's spherical vortex (for which $\epsilon = \sqrt{2}$). Equating the above equations to the corresponding scaled relations in Norbury's analysis, and considering circulation, impulse and energy conserved, Mohseni and Gharib found the following equation:

$$\frac{L_m}{D_0} = \sqrt{\frac{\pi}{2}} \frac{I_R^{1/2} \Gamma_R^{3/2}}{E_R}. \tag{13}$$

Similary, Linden and Turner found

$$\frac{W}{U_p} = \frac{W_R I_R}{2 E_R}, \tag{14}$$

where $W = U_v$ is the propagation velocity of the ring. The values Γ_R, E_R, I_R and W_R are available in tabulated form for different mean core radii ϵ in Norbury's paper [39]. Figure 11 shows the ratio between the velocity propagation and the ejection velocity as a function of ϵ. The values are in the range $0.4 < W/U_p < 0.7$ which compare very well with the vortex velocities shown in Fig. 7 for $Re_0 = 260$ and $L_m/D_0 > 4$; our velocities are in the range $0.5 < U_v/U_p < 0.7$ before the decay. Figure 11 also shows the limit stroke ratio L_m/D_0 as a function of ϵ. The maximum value of L_m/D_0 above which a single ring cannot be formed is $L_m/D_0 = 7.83$. This limit corresponds to Hill's spherical vortex. For a parabolic input velocity profile, Linden and Turner [18] proposed corrections to the constants of the slug flow Eqs. (9)–(11). Using the same procedure, they found that the maximum plug length is reduced by a factor of 0.43, that is, the $(L_m/D_0)_{\text{lim}}$ corresponding to Hill's vortex would be 3.39.

Figure 11 indicates that it is possible to increase the value of the critical stroke ratio if the vortex size increases too. Mohseni and Gharib [37] suggested that thicker vortex rings could be generated using a cylinder with a time-varying exit diameter during formation; therefore, the formation number could be delayed to higher values. The above was confirmed experimentally by Dabiri and Gharib [19]; they found that the vortex ring pinch-off could be delayed up to $L_m/D_0 = 8$. Mohseni et al. [14] showed that the pinch-off could be delayed

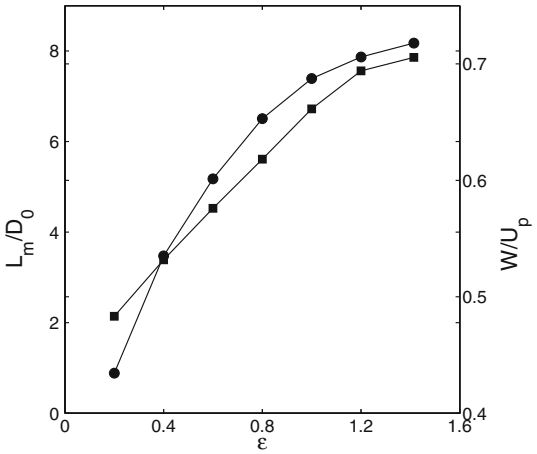

Fig. 11 Critical stroke ratio (*filled squares*) and non-dimensional propagation velocity (*filled circles*) against non-dimensional mean core radius. Taken from Linden and Turner [18]

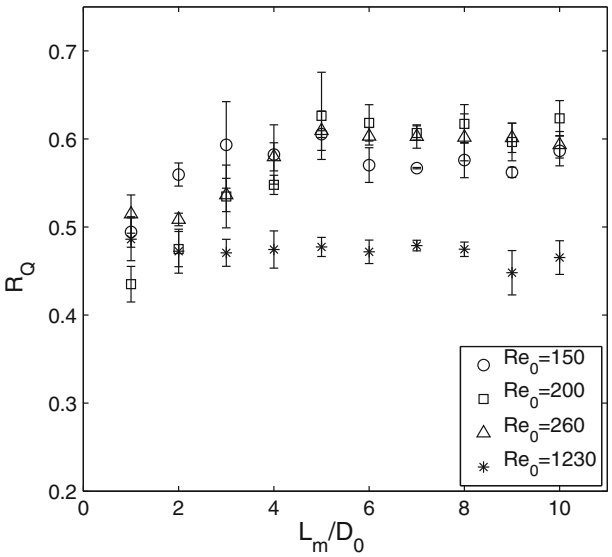

Fig. 12 Non-dimensional radius (Eq. (15)) for different Reynolds numbers

($L_m/D_0 > 4$) if the trailing shear layer accelerates relative to the forming vortex ring so that the shear layer energy was sufficient to be accepted by the vortex ring making them thicker (closer to Hill's spherical vortex).

In Fig. 10 we observe that for $Re_0 = 150$ the limit stroke ratio at which the vortex circulation reaches a maximum is close to $L_m/D_0 \approx 4$. For this Reynolds number we also observe that for $2 \leq L_m/D_0 \leq 4$ the vortex circulation appears to be larger than the other cases. This fact may indicate that it is also possible to generate thicker vortices as Re_0 decreases. To verify this possibility, we measured the vortex ring radius based on the definition of ϵ (Eq. (12)). We define the non-dimensional radius as:

$$R_Q^2 = \frac{A_Q}{\pi R_v^2}, \tag{15}$$

where $R_v = D_v/2$ is the distance between the maximum point of curvature and the axis of symmetry ($y = 0$). As mentioned before, we consider the vortex ring area as A_Q: the region of flow where $Q > 0$, which is also the region within which we calculated the vortex ring circulation. Figure 12 shows the non-dimensional radius R_Q as a function of L_m/D_0 for three low Reynolds numbers and one with high Re_0 (for comparison). The non-dimensional radius is computed when the maximum vortex ring circulation is achieved. For low stroke ratios, $R_Q \approx 0.5$. We can observe that for low Reynolds numbers R_Q increases until it reaches a value close

to $R_Q = 0.6$. In order to make a comparison, we included in this graph the values of R_Q for vortex rings with $Re_0 = 1230$ (using water). In this case, we observe that the non-dimensional radius is close to $R_Q = 0.47$ which are lower values than those for $Re_0 \sim$ O(100). Based on these observations, we can conclude that the size of the vortex rings (measured as R_Q) increases as Re_0 decreases. For this range of Re_0, the vortices are capable of growing "thicker." More circulation can be fed in their cores, reaching a size close to that of a Hill's vortex. The Norbury radius ϵ obtained analytically by Mohseni and Gharib [37] for the *pinch-off* process (and inviscid flow) is $\epsilon \approx 0.35$. This value is indeed smaller than those reported here for $Re_0 \sim$ O(100). Note, however, that our method to obtain an experimental non-dimensional radius (R_Q) is different and perhaps, direct comparisons are not appropriate.

For the case of Gharib et al. [13], the *formation number* is equal to the formation time for which total circulation reaches a value equal to the leading vortex (see, e.g., their Fig. 12). The computation of this number requires a *pinch-off* process (according to Gharib et al. a physical separation of the vortex). We have found that the main difference for small Re_0 is that such separation does not occur, at least considering the procedure proposed by Gharib et al. . Hence, to study the maximum amount of circulation that a vortex in a low Re_0 flow could attain, we had to adopt a different criterion. We considered the maximum circulation value for each stroke ratio regardless of the distance at which this value is reached. It is important to note that the computation of the maximum circulation shown in Fig. 10 is not necessarily an indicator of the "pinch-off" process. Furthermore, the critical stroke ratio presented here does not represent the "formation number" defined by Gharib et al. . For low Reynolds numbers, vorticity dissipation is important. As the vortex ring is forming, it gains circulation from the initial jet; however, this circulation may also be dissipated at the axis of symmetry. In other words, vortex rings may grow up until the point when the circulation is canceled. In fact, we think that for large L_m/D_0 the maximum circulation is reached before the piston has finished its motion.

Our results from Fig. 10 are comparable with Fig. 6 from Gharib et al. [13] and Fig. 9 from Rosenfeld et al. [15] where circulation is plotted as a function of the maximum stroke ratio L_m/D_0. Rosenfeld et al. presented the non-dimensional circulation of vortex rings at a formation time of $t^* \approx 10$ when physical separation is visible. Their numerical calculations reported that the maximum vortex ring circulation is reached when $4 \leq L_m/D_0 \leq 6$. Despite the difference in the maximum circulation value for low Reynolds number and a different criterion, we obtained critical stroke values in close agreement with those reported by Gharib et al. [13] and Rosenfeld et al. [15].

6 Concluding remarks

The main objective of this study was to conduct experiments to analyze the formation of vortex rings at Reynolds numbers of O(100). To our knowledge, measurements in this range of Re_0 do not exist in the specialized literature. To find the conditions at which vortices are formed, we had to consider an identification scheme which was different from what had been used for flows at higher Re_0. We proposed the use of the so-called Q criterion to identify and measure the vortex strength. We used a calculation of the curvature of Lagrangian trajectories to locate the vortex centers. These techniques were used to analyze the formation for vortices in a range of Re_0 from 150 to 260. The same qualitative trend reported by previous investigations was found; the critical stroke ratios for the Reynolds numbers studied are in the range ($4 \leq L_m/D_0 \leq 6$).

By measuring the non-dimensional radius R_Q of the vortex rings, we showed that the vortices with low Re_0 are "thick." According to our observations, such thick vortices can attain more vorticity and have more circulation.

We observed that the vortex ring circulation (for our Reynolds numbers) changes continuously during the formation and propagation of the vortex rings. As the circulation does not remain constant, the impulse, energy and, consequently, the propagation velocity change as well. The measurements of vortex ring diameter and velocity propagation indicate that there is a stroke ratio limit above which the vortex size and velocity cannot increase. The vortex identification scheme used in this paper allows us to obtain measurements of the circulation in the core of the vortex rings with small uncertainty, since the same cutoff criterion can be used at any instant of the vortex ring formation, any distance from the exit and any Reynolds number. The experimental results are in agreement with the theoretical models and numerical studies reported in the literature. Our results confirm the existence of a critical stroke ratio for Re_0 of O(100).

Acknowledgments Authors would like to thank Ian Monsivais for his help in the laboratory. We are also grateful to the Dirección General de Estudios de Posgrado (DGEP-UNAM) for granting C.A.P.-M. a doctorate scholarship. The support of CONACyT (grant 102527) is gratefully acknowledged.

References

1. Shariff, K., Leonard, A.: Vortex rings. Ann. Rev. Fluid Mech. **24**, 235–279 (1992)
2. Lim, T.T., Nickels, T.B.: Vortex rings. In: Green S.I. (ed.) Fluid Vortices, Kluwer Academic Publishers, Berlin, pp. 95–153. (1995)
3. Anderson, E.J., Demont, M.E.: Jet flow in steadily swimming adult squid. J. Exp. Biol. **208**, 1125–1146 (2005)
4. Bartol, I.K., Krueger, P.S., Stewart, W.J., Thompson, J.T.: Pulsed jet dynamics of squid hatchlings at intermediate Reynolds numbers. J. Exp. Biol. **212**, 1506–1518 (2009)
5. Bartol, I.K., Krueger, P.S., Thompson, J.T.: Hydrodynamics of pulsed jetting in juvenile and adult brief squid Lolliguncula brevis: evidence of multiple jet modes and their implications for propulsive efficiency. J. Exp. Biol. **212**, 1889–1903 (2009)
6. Dabiri, J.O., Colin, S.P., Costello, J.H.: Fast-swimming hydromedusae exploit velar kinematics to form an optimal vortex wake. J. Exp. Biol. **209**, 2025–2033 (2006)
7. Gharib, M., Rambod, E., Kheradvar, A., Sahn, D.J.: Optimal vortex formation as an index of cardiac health. Proc. Natl. Adad. Sci. USA **103**, 6305–6308 (2006)
8. Querzoli, G., Falchi, M., Romano, G.P.: On the flow field generated by a gradually varying flow through an orifice. Eur. J. Mech. B Fluid. **29**, 259–268 (2010)
9. Maxworthy, T.: Some experimental studies of vortex rings. J. Fluid Mech. **81**, 465–495 (1977)
10. Didden, N.: On the formation of vortex rings: rolling-up and production of circulation. Z. Angew. Mech. Phys. **30**, 101–116 (1979)
11. Glezer, A., Coles, D.: An experimental study of a turbulent vortex ring. J. Fluid Mech. **211**, 243–283 (1990)
12. Weigand, A., Gharib, M.: On the evolution of laminar vortex rings. Exp. Fluids **22**, 447–457 (1997)
13. Gharib, M., Rambod, E., Shariff, K.: A universal time scale for vortex ring formation. J. Fluid Mech. **360**, 121–140 (1998)
14. Mohseni, K., Ran, H., Colonius, T.: Numerical experiments on vortex ring formation. J. Fluid Mech. **430**, 267–282 (2001)
15. Rosenfeld, M., Rambod, E., Gharib, M.: Circulation and formation number of laminar vortex rings. J. Fluid Mech. **376**, 297–318 (1998)
16. Dabiri, J.O., Gharib, M.: Delay of vortex ring pinch-off by an imposed bulk counter-flow. Phys. Fluids **16**, L28–30 (2004)
17. Krueger, P.S., Dabiri, J.O., Gharib, M.: The formation number of vortex rings formed in uniform background coflow. J. Fluid Mech. **556**, 147–166 (2006)
18. Linden, P.F., Turner, J.S.: The formation of optimal vortex rings, and the efficiency of propulsion devices. J. Fluid Mech. **427**, 61–72 (2001)
19. Dabiri, J.O., Gharib, M.: Starting flow through nozzles with temporally variable exit diameter. J. Fluid Mech. **538**, 111–136 (2005)
20. Jeong, J., Hussain, F.: On the identification of a vortex. J. Fluid Mech. **285**, 69–94 (1995)
21. Haller, G.: An objective definition of a vortex. J. Fluid Mech. **525**, 1–26 (2005)
22. Chakraborty, P., Balachandar, S., Adrian, R.J.: On the relation between local vortex identification schemes. J. Fluid Mech. **535**, 189–214 (2005)
23. Hunt, J.C.R., Wray, A., Moin, P.: Eddies, stream, and convergence zones in turbulent flows. Center for Turbulence Research Report CTR-S88 (1988)
24. Chong, M.S., Perry, A.E., Cantwell, B.J.: A general classification of three-dimensional flow fields. Phys. Fluids A **2**, 765–777 (1990)
25. Okubo, A.: Horizontal dispersion of floatable trajectories in the vicinity of velocity singularities such as convergences. Deep Sea. Res. **17**, 445–454 (1970)
26. Weiss, J.: The dynamics of entrophy transfer in 2-dimensional hydrodynamics. Phys. D **48**, 273–294 (1991)
27. Oullette, N.T., Gollub, J.P.: Curvature fields, topology, and the dynamics of spatiotemporal chaos. Phys. Rev. Lett. **99**, 194502 (2007)
28. Braun, W., Lillo, F.de , Eckhardt, B.: Geometry of particle paths in turbulent flows. J. Turbul. **7**, 62 (2006)
29. Willert, C., Gharib, M.: Digital particle image velocimetry. Exp. Fluids **10**, 181–193 (1991)
30. Raffel, M., Willert, C., Kompenhans, J.: Particle Image Velocimetry. A practical guide. Springer, Berlin (1998)
31. Ozcan, O., Meyer, K.E., Larsen, P.S.: Measurement of mean rotation and strain rate tensors by using stereoscopic PIV. Exp. Fluids **39**, 771–783 (2005)
32. Holman, J.P.: Experimental Methods for Engineers, 6th edn. McGraw-Hill, New York (1994)
33. Lourenco, L., Krothapalli, A.: On the accuracy of velocity and vorticity measurements with PIV. Exp. Fluids **18**, 421–428 (1995)
34. Dabiri, J.: Optimal vortex formation as a unifying principle in biological propulsion. Ann. Rev. Fluid Mech. **41**, 17–33 (2009)
35. Michalke, A., Timme, A.: On the inviscid instability of certain two-dimensional vortex-type flows. J. Fluid Mech. **29**, 647–666 (1967)
36. Shetty, S., Assay-Davis, X., Marcus, P.: On the interaction of Jupiter's great red spot and zonal jet streams. J. Atmos. Sci. **64**, 4432–4444 (2007)
37. Mohseni, K., Gharib, M.: A model for universal time scale of vortex ring formation. Phys. Fluids **10**, 2436–2438 (1998)
38. Fraenkel, L.E.: Examples of steady vortex rings of small cross-section in an ideal fluid. J. Fluid Mech. **51**, 119–135 (1972)
39. Norbury, J.: A family of steady vortex rings. J. Fluid Mech. **57**, 417–431 (1973)